AN ASSESSMENT OF VEERING WIND EFFECTS ON SCATTEROMETRY FROM THE SEA SURFACE

LARRY F. BLIVEN
NASA/Goddard Space Flight Center
Laboratory for Hydrospheric Processes
Wallops Island, VA 23337 USA

VALERIE BILLAT
Universities Space Research Association
Goddard Space Flight Center
Greenbelt, MD 20771 USA

PIOTR W. SOBIESKI and ALBERT GUISSARD
Université Catholique de Louvain
Département d'Electricité
B-1348 Louvain-la-Neuve, Belgium

HUBERT BRANGER and JEAN-PAUL GIOVANANGELI
Institut de Mécanique Statistique de la Turbulence
12 Av Général Leclerc, Marseille, France

Abstract. To characterize scatterometer returns from the sea surface near meteorological fronts, we investigated microwave scattering from seas in which long waves are at oblique angles to short waves. We simulate the effects of veering winds on C- and K_u-band scatterometers by using models in which the short waves align with the wind friction velocity u_*, but the long waves are at oblique angles to the u_* direction. The analysis reveals two main effects due to the rotation of the long wave slope probability density distribution. Azimuthally averaged normalized radar cross section a_0 decreases as the oblique angle increases. Additionally, two regimes exist. In the small angle regime, azimuthal scans of normalized radar cross section σ° exhibit features similar to the classic double-maxima pattern for non-veering wind conditions, but the axis of σ° maxima is rotated toward the long wave axis. In the large angle regime, more than two maxima are apparent in azimuthal scans. Therefore it maybe inappropriate to use standard three term Fourier cosine models for some veering wind conditions

The *International Journal of Remote Sensing*,
1995. **Vol. 16, No. 5**, 891-903.

Homepage: bliven2.osb.wff.nasa.gov
Email: bliven@osb.wff.nasa.gov
Office Phone:757-824-1057

1. Introduction

Scatterometer backscattered power data are typically useful to infer wind vectors by analysis of normalized radar-cross-section scans $\sigma^{\circ}(\mathbf{v}, \phi, \theta)$, where $\mathbf{v}$ is the wind vector, and ϕ and θ are the radar azimuthal and incidence angles. For suitable steady conditions, wind-wave distributions of the sea surface are symmetric with respect to the average wind direction, so azimuthal scans of σ° are well described by three-term Fourier cosine models (Ulaby *et al.* 1982). Steady winds, however, do not persist indefinitely because weather conditions are nonstationary, with notable gradients near meteorological fronts and major cyclones. Short waves rapidly adjust to the local wind conditions but the relaxation time for long waves is prolonged; consequently, wave distributions are not always symmetric with respect to the local wind direction. Thus for veering winds, the energy-containing long waves are not aligned with the wind vector and unfortunately there is a dearth of field measurements to characterize σ°. If operational scatterometer algorithms do not account for these circumstances, there is a possibility of increased errors in wind vector estimates in regions where the weather is changing rapidly. Fronts are of considerable meteorological and oceanic interest, so it is important to understand and to monitor air-sea interaction processes in these areas. The objective of this paper is to present results of numerical simulations that we conducted to assess the likely effects of veering winds.

Wave models depicting seas generated by homogeneous steady winds will be used as the basis for comparison. The elevation spectra that we used each have a single peak and all the spectral components are symmetrically distributed with respect to the wind vector. Many numerical models characterize the development of surface waves using a net source function, which is composed of input S_{in}, nonlinear transfer due to resonant wave-wave interactions S_{nl}, and dissipation S_{ds}. S_{in} is dominated by air-sea momentum fluxes that rapidly generate short waves, which reach an equilibrium size that is dependent upon the local wind forcing, small-scale wave breaking and wave-wave interactions. S_{nl} redistributes energy from small waves to large waves. Whitecapping limits the size of long waves and it is the dominant component of S_{ds}. For fetch or duration limited conditions, spectral evolution proceeds with a gradual development of longer wave components, such that the total wave energy increases as the spectral peak shifts to longer waves. This continues until conditions reach the fully developed state, for which wind input is locally balanced by dissipation and the spectral shape is only dependent upon the local wind.

Now consider the effects of veering winds. From an examination of data and numerical models (Hasselman *et al.* 1980, Günther *et al.* 1981, Allender *et al.* 1983, Holthuijsen *et al.* 1987, Young *et al.* 1987, Van Vledder and Holthuijsen 1993, Quanduo and Komen 1993), we find that a congruous description emerges. Assume that homogeneous steady winds are the existing conditions, when suddenly the wind shifts, without changing speed, to a different direction. High frequency waves are closely coupled to the air boundary layer and they adjust quickly, order of minutes, to new conditions; however the relaxation time for low frequency waves is in the order of hours. So by 'veering' or 'rapidly turning' winds, we mean that the wind direction changes by a significant amount in an interval that is short compared to that required for complete angular relaxation of the entire wave-field. Two regimes are observed: a small shift regime and a large shift regime. In the large shift regime, the wind direction rotates by more than about 60 to 90^{o} and a new independent wave system is generated following classical trends, while the preexisting wave system dissipates. This study considers just the small shift regime, in which the wind rotates by less than about 60 to 90^{o} and the

existing long-wave spectrum slowly rotates to the new wind direction. High-frequency waves quickly align with the effective wind stress; nonlinear interactions siphon energy away from the new wave system (therefore retarding development of a secondary peak) and transfer energy to the preexisting long wave system; and long waves lose energy through whitecapping. Due to the asymmetric energy gains by radiative effects and energy losses due to dissipation, the long-wave system slowly rotates toward the new wind direction. The rotational relaxation time is approximately equal to the development time for fully developed seas at comparable wind speed; the rotational relaxation-time, however, is sensitive to wave-age (shorter for fresher seas). Therefore in small shift cases, spectral evolution due to veering winds results in rapid adjustment of short waves to the new wind direction and subsequent turning of long waves.

To study how these factors affect remote sensing measurements, we conducted a numerical experiment with C- and Ku-band scatterometers. The sea-surface models and scattering computations are reviewed in section 2 and the findings are presented in section 3. This analysis reveals that long waves at oblique angles to short wind-generated waves would contribute to considerable errors in wind vectors inferred from scatterometer data.

2. Methods

The UCL simulator was used in this study to compute backscattered microwave power values for C- and K_u-band scatterometers. This software was developed to aid in altimeter and scatterometer investigations and it is thoroughly documented by Sobieski *et al.* (1986); concisely reviewed by Guissard *et al.* (1994) and Sobieski *et al.* (1994); and particular features reported by Baufays *et al.* (1988 a&b), Guissard *et al.* (1986, 1987, 1989) and Sobieski *et al.* (1991, 1993). Maxwell's equations are the fundamental equations of electromagnetic theory, which is the basis for these estimates of backscattered microwave power from wind-generated surface waves. As is usually done, the UCL simulator uses composite surface theory, which was developed to deal with the large surface displacements found in ocean waves. A thorough review of this approach is presented by Plant (1990). Although various approximations are required, an important one is that for incidence angles between about 20 and 70^o, the primary effect of the large-scale surface is simply to tilt the small-scale structure which backscatters according to first-order Bragg theory. Guissard (1993) clarified differences between sea surface models used for wave propagation studies and models used for scattering studies. Because there is no sea surface model that is universally accepted as the standard for naturally occurring winds and seas, we will summarize the ones that we selected. This modelling assumes a spatially homogeneous wave field over a scatterometer footprint.

Diverse sea surface models can be used in the UCL simulator, as long as we can represent the two-dimensional wavenumber amplitude spectrum ψ as

$$\psi(k, \phi_k) = \chi(k)\, F(k, \phi_k), \qquad \textbf{(1)}$$

where $\chi(k)$ is a radial spectrum and $F(k,\phi_k)$ is an angular factor.

To represent a broad range of sea states from a minimum of input parameters, we employed two radial spectral models: for fully arisen seas, the Bjerkaas and Riedel (1979) spectrum $\chi^{BR}(k)$; and for nonfully developed seas, the Wallops-Toba-Cox spectrum $\chi^{WTC}(k)$ of Guisssard *et al.* (1994). These models are composed of distinct segments. Long waves (the dominant component of the surface displacement) are dependent upon wind conditions in the χ^{BR} model; that portion of the spectrum

is independent of wind conditions in the χ^{WTC} model. On the other hand, the short waves which are strongly coupled to the wind have the same representation in χ^{BR} and χ^{WTC}, i.e., the Toba (1973) model for short gravity waves and the Cox (1958) model for gravity-capillary waves. For each spectrum, the transitional wavenumbers between sections match spectral densities between sections. Consequently, transitional wavelengths vary with the physical conditions; however, transition from long waves to the Toba region occurs at wavelengths between about one-forth and one-twentieth of the peak wavenumber. Thus there is no convergence problem in computations of the Bragg scattering component for veering cases because the spectral region is sufficiently broad around the resonant wavelengths of the C- and K_u-band scatterometers. Like previous models of veering wind seas, this simulation relates small-scale sea-surface features to wind stress by using scaling relationships derived for non-veering conditions. The validity of this assumption (as well the dependence of the surface stress on the wind field) should be examined (Ly, 1993), but these issues are beyond the scope of this study. Together the χ^{BR} and χ^{WTC} models are useful for analysis of a wide range of sea states and thus we adopted them for this veering wind study by altering the angular factor.

The angular factor that we use is

$$F(k, \phi_k) = \frac{1}{2\pi}[1 + d_1 \cos(2\phi - \Omega(k))], \qquad \textbf{(2)}$$

where d_1 is determined using along- and cross-wind slope variances as specified by Cox and Munk (1954). ϕ is the direction relative to the wind direction and Ω is an offset angle to account for veering effects. This angular factor is consistent with the main features contained in the three-term Fourier cosine formulation. For non-veering conditions, all the wave components are symmetrically distributed about the mean wind axis, so Ω is always equal to 0^o. On the other hand for veering cases, Ω is 0^o for the Toba-Cox spectral regions, but for long waves, Ω is the oblique angle that corresponds to the wind rotation. The simulation results are dependent upon the angular factor, which needs further investigation for veering conditions. Because long waves tend to retain their size and spreading characteristics from prior to wind shifts, we assume that tilt factors accounted for by the large scale slope probability density distributions P_{LS} are unchanged by wind shifts, except that each P_{LS} is rotated by Ω with respect to wind direction. We characterize each P_{LS} by the non-Gaussian model for clean water derived from field data by Cox and Munk (1954). P_{LS} enters the computation of both the specular and Bragg scattering terms, so to assure precision (convergence to 0.1%), both terms are computed to obtain the total backscattered power; however, the Bragg term is the dominant one contributing to the backscattered power for the range of simulated conditions.

3. Results

Baseline conditions for fully developed seas are presented, then we assess (a) the effects of veering winds ensuing fully developed seas and (b) the sensitivity of the veering wind effects to the size of the long-wave slope. Both 5.3 and 13.5 GHz scatterometers were simulated because they represent systems that continue to be of interest for space applications. Because the trends are similar, only C-band figures are presented.

3.1. Baseline conditions

Fully developed seas depend on just the local wind and consequently models of fully developed seas provide a useful choice for baseline conditions. Azimuthal scans of scatterometer returns from the sea surface are ordinarily well correlated with surface wind vectors, so the wind vector is the principal parameter inferred from scatterometer measurements.

The fully developed state of the sea is often modeled using the Pierson-Stacy radial spectrum (Pierson and Stacy, 1973), as modified by Bjerkaas and Riedel (1979). With χ^{BR} selected in the UCL simulator, we computed σ^o for various wind speeds and viewing angles. The wind speed dependence of azimuthal scans from a 5.3 GHz scatterometer that we call C-SCATT (VV polarization) are shown in figure 1 for incidence angles of 30^o and 45^o. The scans exhibit features in common with *in situ* measurements, i.e., power levels increase as friction velocity increases and the maxima for each scan align with the along wind axis ($\phi = 0$ and 180^o).

The azimuthal variation of σ^o is usually described by a three-term cosine series as

$$\sigma^o = a_0 + a_1 \cos(\phi) + a_2 \cos(2\phi). \qquad \textbf{(3)}$$

Each coefficient depends on wind speed, incidence angle and microwave polarization. If ϕ is chosen to be 0^o for the scatterometer pointing upwind and if the scans have positive symmetry about the axis of the average wind direction, then this formulation is effective because the physical interpretation of the coefficients is straight forward. a_0 is the azimuthally averaged cross-section and it is an increasing function of u_*; a_1 is a measure of upwind/downwind asymmetry and a_2 is the upwind/crosswind modulation. a_1 values are small compared to a_0 and a_2, so many operational algorithms neglect it. For wind retrieval from ERS-1 scatterometer data, a_1 is included in an inversion algorithm by Stoffelen and Anderson (1993), however, its magnitude can be comparable to the instrumental noise and therefore it is not always useful. Fortunately, the 180^o wind direction ambiguity can be removed through consideration of the large-scale wind field that is provided by forecast winds from weather centers. Several processes that are not well understood contribute to upwind/downwind asymmetry. In this simulation, the dominant component of the small upwind/downwind asymmetry arises from the non-Gaussian long wave slope probability density model P_{LS}. Hydrodynamic effects and air-sea boundary effects can also contribute to a_1 (Plant, 1986). Those processes are not included here. They are left to future refinements when more is known about the partitioning of the asymmetry among the various sources. For baseline conditions, u_* is inferred from the size of a_0 and the wind-stress axis coincides with the axis of the maxima in the azimuthal scans.

To assess veering wind effects that could cause serious errors with respect to baseline conditions, we used data such as that in figure 1 to develop empirical relationships between u_* and a_0. The selection of a functional relationship between the variables is subject to investigator preference. Power-law relationships, such as that employed for the K_u-band scatterometer on SEASAT (Schroeder *et al.* 1982), have great appeal because of their relative ease for operational usage. Unfortunately an error analysis by Woiceshyn *et al.* (1986) shows that the single power-law model did not uniformly meet SEASAT system specifications and because biases occurred at both low and high winds, they recommended that a two-segment power-law be used. We find that second-order polynomial models fit the entire range of simulated data well and were convenient to use for the error analyses that are presented later. As an example, for baseline conditions with C-SCATT at incidence angle of 30^o, the wind-speed dependence is well represented ($r^2 > 0.999$) by

$$u_*(cm\ s^{-1}) = -0.614 + 354 a_0 - 357 a_0^2, \quad \textbf{(4)}$$

where a_0 is normalized backscattered power (not dB).

3.2. Veering wind effects ensuing fully developed seas

Let's appraise situations in which the wind changes direction, with speed unchanged. Due to geometrical symmetry, clockwise and counterclockwise veering winds yield scatterometric scans that are mirror images, so we present only counterclockwise wind-shifts. Starting with each baseline wind speed, we computed azimuthal scans for veering winds with Ω ranging from 0 to 55°, by 5°. Figure 2 presents a typical example for u* = 30 cm s^{-1}, corresponding to about 8 m s^{-1} surface winds. The scatterometer points upwind for $\phi = 0°$, so counterclockwise veering winds appear as clockwise rotations of long waves. The scans show that (a) σ° decreases as the veering angle increases, (b) maxima are rotated away from the wind axis and toward the long-wave axis and (c) at large veering angles, a regime exists with more than two maxima per scan.

Veering winds reduce power levels in azimuthal scans of C-SCATT, so we assessed the size of wind speed biases that could occur if baseline algorithms for fully developed seas are employed. The relative error of wind speed estimates due to veering winds was computed as

$$\Delta = \frac{u_*(\Omega) - u_*}{u_*}, \quad \textbf{(5)}$$

where $u_*(\Omega)$ is the friction velocity inferred by using a baseline algorithm with input a_0 from a veering-wind azimuthal scan. We summarize the results in figure 3, which shows the relative error increasing more rapidly for higher winds and for larger incidence angles. Typical operational design specifications call for less than 10% error in wind estimates. So the errors meet design objectives for Ω less than about 20°. On the other hand, at larger angles the friction velocity estimates are grossly underestimated. Notice that for some conditions, the reduction of a_0 is so large that a scan might be interpreted as representing calm wind.

The classic three-term Fourier cosine model is not really appropriate when there are more than two maxima per scan. Therefore for each wind speed and incidence angle, as the veering angle increases, a critical angle exists beyond which the model produces dubious directional information. For the study conditions, figure 4 shows that the critical angle ranges from about 12 to 40°. We classify scans into the small angle regime if there are two maxima per scan, otherwise into the large angle regime. For each C-SCATT configuration, the critical angle is well represented as a linear function of u_*. The transition between regimes occurs at smaller critical angles for (a) lighter winds and (b) larger incidence angles.

3.3. Nonfully developed sea

Nonfully developed seas are associated with rising and falling seas due to fetch and duration limited wind conditions. During rising seas the dominant waves tend to be steeper than those of fully developed seas, whereas the energy-containing waves are more gentle in falling seas. Normally with all waves aligned, the effects of long-wave tilt on backscattered power are such that if a radar footprint is small compared to the dominant wavelength, the variability is large within the data set; but in terms of average values (from time-series or large radar footprints), the effect of long-wave variability is second order. For steady winds blowing off-shore at > 7 m s^{-1}, Ross and Jones (1978) obtained data from an aircraft-borne 13.9 GHz scatterometer and conclude that interactions between large and small-scale structure produce relatively small changes in mean values of σ°. A recent analysis by Sobieski *et al.* (1994) shows that the effects of long-wave tilt variability on σ° are more apparent at lighter winds. In this section, the importance of long-wave slope variability is assessed in terms of wind estimates by using C-SCATT for non-veering and veering winds.

In order to study the nonfully developed state of the sea, Guissard *et al.* (1994) developed the Wallops-Toba-Cox model. In χ^{WTC}, large-scale waves are represented by the Wallops model of Huang *et al.* (1981), hence the spectral section representing the dominant energy-containing waves is dependent upon two parameters: the significant slope δ and the peak wavenumber k_p. δ is defined as

$$\delta = \frac{\zeta_d}{\lambda_p} \quad . \qquad \textbf{(6)}$$

ζ_d is the rms value of the vertical displacement. λ_p is that particular wavelength that is related to the peak frequency ω_p of the sea-surface frequency spectrum by the wave dispersion relationship for deep-water gravity waves ($\omega^2 = gk$). In this last expression, k is the wavenumber and g is the acceleration of gravity. χ^{WTC} is a function of three parameters (δ, k_p and u_*), so a complete parametric analysis of all conceivable conditions is beyond the scope of this study. Consequently we will simply demonstrate some trends by choosing (a) k_p from the χ^{BR} formulation, i.e. $k_p = g/U_{19.5}^2$ where $U_{19.5}$ is the wind speed at 19.5 m; and (b) a range of δ varying from 0.004 to 0.012. Because δ = about 0.0083 for fully developed seas, this analysis includes rising and falling seas.

For non-veering conditions with a moderate wind of u_* = 30 cm s^{-1}, let's examine the importance of long-wave steepness on C-SCATT. Figure 5 shows azimuthal scans and it is apparent that the variability of σ° attributable to δ is detectable at an incidence angle of 30°, but it is almost imperceptible at 45°. To gain insight into the importance of this effect, we computed the relative error of friction velocity estimates for a broad range of wind speeds and the results are shown in figure 6. For this error analysis, $u_*(\delta)$ is the friction velocity inferred by using a baseline algorithm developed for $u_*(\delta=0.0083, k_p \text{ of } \chi^{BR})$. The uncertainty of u_* attributable to δ variability is barely detectable at an incidence angle of 30° and hardly discernable at 45°. Because all the errors are less than 10 %, the effects of long wave steepness on C-SCATT are practically inconsequential for these nonveering conditions. This result is consistent with previous assessments, e.g. by Valenzuela (1968) and Durden and Vesecky (1985).

On the other hand, veering wind effects can be very important for both rising and falling seas. See for example the C-SCATT azimuthal scans for falling seas in figure 7. Even for this gentle sea

example, the scans illustrate that the effects of veering winds are notable at both incidence angles. In order to see the importance of veering-winds for a broad range of rising and falling seas, we computed the relative error of u_* estimates for the 30 cm s^{-1} case. For this analysis, we developed a baseline wind speed algorithm for each δ to isolate the errors to just veering effects. Figure 8 displays the results, which are (a) that errors due to veering winds increase as δ increases and (b) that regardless of incidence angle and δ, considerable errors are encountered as the veering angle increases.

These results for rising and falling seas indicate that long wave alignment needs to be addressed to develop enhanced data inversion algorithms for scatterometers. Models that account for long wave slope, but not long wave alignment, are not suitable for veering wind conditions.

4. Summary

This study provides an assessment of veering wind effects on wind estimates from scatterometry of the sea surface. Results from the numerical experiment with C- and K_u-band scatterometers reveal that veering winds reduce backscattered power levels and alter the shape of azimuthal scans. The anomalies are comparable for both frequencies, so irregularities can not be significantly reduced by selecting a C- or K_u-band scatterometer. On the other hand, studies are needed to develop techniques to improve wind estimates for veering conditions, and the usual factors such as hardware costs and reliability ought to be evaluated for selection of microwave frequencies for satellite systems. Fortunately if the veering angle is less than about $\pm 20^o$, the errors due to veering winds should be within typical design specifications (± 10 % for magnitude, $\pm 20^o$ for direction). If on the other hand $\pm 20^o < \Omega < \pm 55^o$, the effects of veering winds are dramatic and not negligible so there is more uncertainty in deriving the stress. The general trends appear regardless of long wave steepness or wind speed, so when weather patterns cause a shift in wind direction greater than about $\pm 20^o$ (on a time scale that is short compared to the long wave relaxation time), results from standard scatterometer data reduction algorithms should be used with prudence.

These findings are dependent upon model assumptions, as is always the case for numerical experiments. Although we used sea surface models that are in accord with present qualitative descriptions, more detailed measurements of sea surface morphology for veering winds would certainly be helpful to guide and validate further numerical model development. Refinement of scattering calculations and data inversion techniques will be dependent upon a better understanding of (a) air-sea coupling processes (b) long wave slope probability density distributions and (c) wave-wave interaction mechanisms. In this vein, a recent study by Geernaert *et al.* (1993) presents progress toward understanding the directional attributes of the ocean surface wind stress vector because it provides *in situ* measurements which are evidence that the stress vector direction is altered (stress vector and wind vector are non-aligned) due to long-wave effects pursuant to veering winds. The role of various physical mechanisms that might contribute to this deviation is, however, still unsettled; so further research is needed to model momentum flux at the air-sea interface with respect to the wind profile and sea surface characteristics. It is suggested that veering wind studies also include microwave scattering measurements so that weather fronts can be accurately monitored globally.

A quality control procedure developed by Stoffelen and Anderson (1993) is being used to validate ERS-1 scatterometer data. The analysis quantifies the coherence of σ° triplets and the three-term transfer function for CMOD4. Their recent findings show that the data are generally consistent with

the CMOD4 wind retrieval algorithm. Over distances of 100-150 km near lows, fronts and tropical cyclones, however, the data frequently do not follow the general distribution of triplets. In these cases, no wind retrieval is attempted. Thus the quality of reported winds is not compromised, but there are occasional gaps. Further study is needed to formulate and validate algorithms suitable for measuring winds near lows, fronts and tropical cyclones. This simulation indicates that directional properties of large waves need to be included in those investigations.

Acknowledgments

Parts of the scattering model were developed at UCL under contracts with the European Space Agency (ESA), whose financial support is acknowledged. Financial support was also provided by the NASA Mission to Planet Earth Program; the Office of Naval Research, Marine Boundary Layer Advanced Research Initiative of the Remote Sensing Program and the Physical Oceanography Program; and the Centre National de la Recherche Scientifique. Claude Klapisz of DEA de Methode physique en télédetection, L'Université de Paris VII helped to coordinate and support this collaboration with V. Billat.

References

ALLENDER, J.H., ALBRECHT, J. and HAMILTON, G., 1983, Observations of directional relaxation of wind sea spectra, *Journal of Physical Oceanography*, **13**, 1519-1525.

BAUFAYS, C., GUISSARD, A. and SOBIESKI, P., 1988, A three degree of freedom description of the ocean surface for microwave remote sensing of wave height and wind friction velocity, *Proceedings of the 4th International Colloquium on Spectral Signatures of Objects in Remote Sensing, Aussois, France.* In **ESA Sp-287**, ESTEC, Noordwijk, The Netherlands, 55-61.

BJERKAAS, A.W. and RIEDEL, F.W., 1979, Proposed model for the elevation spectrum of a wind roughened sea surface, *Technical Memorandum 1328*, JHU/APL, Columbia, MD, USA 31p.

COX, C.S., 1958, Measurements of slopes of high frequency wind waves, *Journal of Marine Research*, **16(3)**, 199-229.

COX, C.S. and MUNK, W.H., 1954, Statistics of the sea surface derived from sun glitter, *Journal of the Marine Research*, **13(2)**, 198-227.

DURDEN, S.L. and VESECKY, J.F., 1985, A physical radar cross-section model for a wind-driven sea with swell, *IEEE Jornal of Oceanic Engineering*, **OE-10(4)**, 445-451.

GEERNAERT, G.L., HANSEN, F., COURTNEY, M. AND HERBERS, T., 1993, Directional attributes of the ocean surface wind stress vector, *Journal of Geophysical Research*, **98(C9)**, 16571-16582.

GUISSARD, A., 1993, Directional spectrum of the sea surface and wind scatterometry, *International Journal of Remote Sensing*, **14(8)**, 1615-1633.

GUISSARD A., BAUFAYS C. and SOBIESKI, P., 1986, Sea surface description requirements of electromagnetic scattering calculations, *Journal of Geophysical Research*, **91(2)**, 2477-2492.

GUISSARD, A. and SOBIESKI, P., 1987, An approximate model for the microwave brightness temperature of the sea, *International Journal of Remote Sensing*, **8(11)**, 1607-1627.

GUISSARD, A., SOBIESKI, P. and BAUFAYS, C., 1989, Microwave remote determination of ocean surface parameters A preliminary analysis, *Microwave radiometry Remote Sensing Applications*, edited by P. Pampaloni, VSP Zeist, the Netherlands, 257-269.

GUISSARD, A., BAUFAYS, C. and SOBIESKI, P., 1994, Fully and nonfully developed sea models for microwave remote sensing applications, *Remote Sensing of the Environment*, **48**, 25-38.

GUNTHER, H., ROSENTHAL, W. and DUNCKEL, M., 1981, The response of surface gravity waves to changing wind direction, *Journal of Physical Oceanography*, **10**, 718-728.

HASSELMANN, D.E., DUNCKEL, M. and EWING, J.A., 1980, Directional wave spectra observed during JONSWAP 1973, *Journal of Physical Oceanography*, **10**, 1264-1280.

HOLTHUIJSEN, L.H., KUIK, A.K. and MOSSELMAN, E., 1987, The response of wave directions to changing wind directions, *Journal of Physical Oceanography*, **17**, 845-853.

HUANG, N.E., LONG, S.R., TUNG, C.C., YUEN, Y. and BLIVEN, L.F., 1981, A unified two parameter wave spectral model for a general sea state, *Journal of Fluid Mechanics*, **113**, 203-224.

LY, L.N., 1993, Effect of angle between wind stress and wind velocity vectors on the aerodynamic drag coefficient at the air sea interface, *Journal of Physical Oceanography*, **23**, 159-163.

PIERSON, W.J. and STACY, R.A., 1973, The elevation, slope and curvature spectra of a wind roughened sea surface, *Final Report CR 2247*, NASA, Washington, 129p.

PLANT, W.J., 1986, A two-scale model of short wind-generated waves and scatterometry, *Journal of Geophysical Research*, **91**, 10735-10749.

PLANT, W.J., 1990, Bragg scattering of electromagnetic waves from the air/sea interface, In *Surface Waves and Fluxes*, edited by G.L. Geernaert and W.J. Plant (Amsterdam: Kluwer Academic Publishers), **2**, 41-108.

QUANDUO, G. and KOMEN, G., 1993, Directional response of ocean waves to changing wind direction, *Journal of Physical Oceanography*, **23**, 1561-1566.

ROSS, D. and JONES, W.L., 1978, On the relationship of radar backscatter to wind speed and fetch, *Boundary Layer Meteorology*, **13**, 133-149.

SCHROEDER, L.C., BOGGS, D.H., DOME, G., HALBERSTAM, I.M., JONES, W.L., PIERSON, W.J. and WENTZ, F.J., 1982, The relationship between wind vector and normalized radar cross section used to derive SEASAT A satellite scatterometer winds, *Journal of Geophysical Research*, **87(C5)**, 3318-3336.

SOBIESKI, P.C., GUISSARD, A., BAUFAYS, C., VAN HOENACKER, D., GUILLAUME, A M. and VAN DER VORST, A., 1986, Study on propagation and inverse scattering, ESA Report 5285/82, ESTEC, The Netherlands, **5 vol**, 977p.

SOBIESKI, P.C., GUISSARD A.,and BAUFAYS, C., 1991, Synergic inversion technique for active and passive microwave remote sensing of the ocean, *IEEE Transactions on Geoscience and Remote Sensing*, **29(3)**, 391-406.

SOBIESKI, P.C., GUISSARD, A., BAUFAYS, C. and SIRAUT, Ph., 1993, Sea surface scattering calculations in maritime satellite communications, *IEEE Transactions on Communications*, **41(10)**, 1525-1533.

SOBIESKI, P.C., GUISSARD, A. and BAUFAYS, C., 1994, Comparison of microwave signatures for fully and nonfully developed sea models, *Remote Sensing of the Environment*, **48**, 39-50.

STOFFELEN, A. and ANDERSON, D.L.T., 1993, ERS-1 scatterometer data characteristics and wind retrieval skill, *Proceedings of first ERS-1 Symposium - Space at the Service of our Environment, Cannes, France*. In **ESA Sp-359**, ESTEC, Noordwijk, The Netherlands, 41-47.

TOBA, Y., 1973, Local balance in the air sea boundary processes. Part III: On the spectrum of wind waves, *Journal of the Oceanic Society of Japan*, **29(5)**, 209-220.

ULABY, F.T., MOORE, K.M. and FUNG, A., 1982, *Microwave remote sensing*, II, (Addison Wesley Publishing Company, Reading, MA, USA).

VALENZUELA, G.R., 1968, Scattering of electromagnetic waves from a tilted slightly-rough surface, *Radio Science*, **3(11)**, 1057-1066.

VAN VLEDDER, G.Ph. and HOLTHUIJSEN, L.H., 1993, The directional response of ocean waves to turning winds, *Journal of Physical Oceanography*, **23(2)**, 177-192.

WOICESHYN, P. M., WURTELE, M.G., BOGGS, D.H., MCGOLDRICK, L.F. and PEREHERYCH, S., 1986, The Necessity for a New parameterization of an Empirical Model for Wind/Ocean Scatterometry, *Journal of Geophysical Research*, **91(C2)**, 2273-2288.

YOUNG, I.R., HASSELMANN, S. and HASSELMANN, K., 1987, Computations of the response of a wave spectrum to a sudden change in wind direction, *Journal of Physical Oceanography*, **17**, 1317-1338.

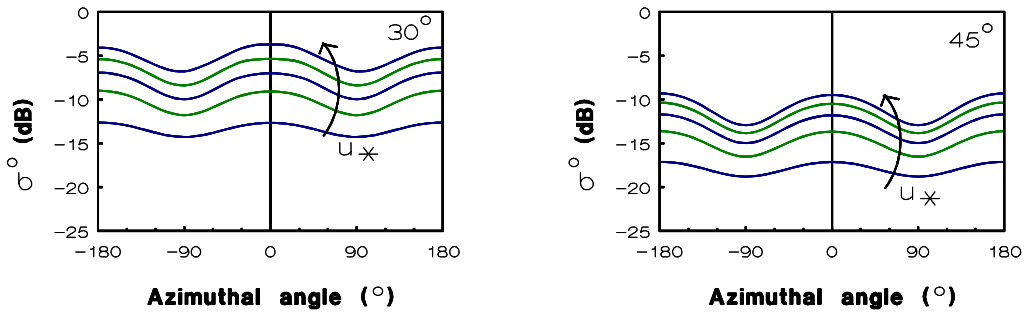

Figure 1. Azimuthal scans from C-SCATT for *fully developed* seas. Subplots a & b in figures 1-8 are for incidence angles of 30 and 45^0. Here u_* ranges from 15 to 75 cm s^{-1} by increments of 15 cm s^{-1}. Scatterometers are normally useful for inferring wind vectors because (a) σ^0 increases as u_* increases and (b) maxima align in the along wind direction.

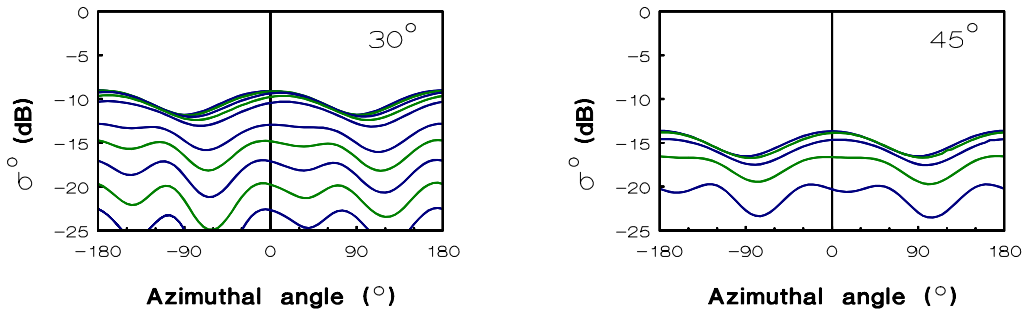

Figure 2. Veering winds ensuing *fully developed* seas cause anomalous effects on C-SCATT scans. This is a moderate wind case with u_* = 30 cm s^{-1}. Starting from the nonveering condition, Ω increments by 5^o per scan. Two effects emerge as Ω increases: σ^0 decreases, and a regime appears with more than two maxima per scan.

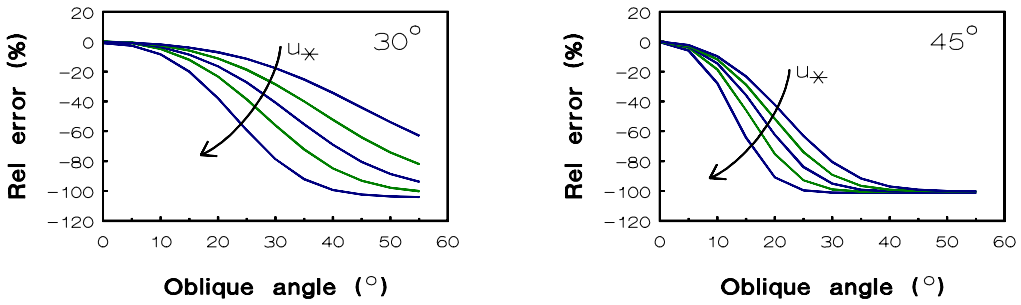

Figure 3. Wind speed errors due to veering winds ensuing *fully developed* seas. u_* is as in figure 1. Regardless of wind intensity, wind speeds are apt to be underestimated as Ω increases.

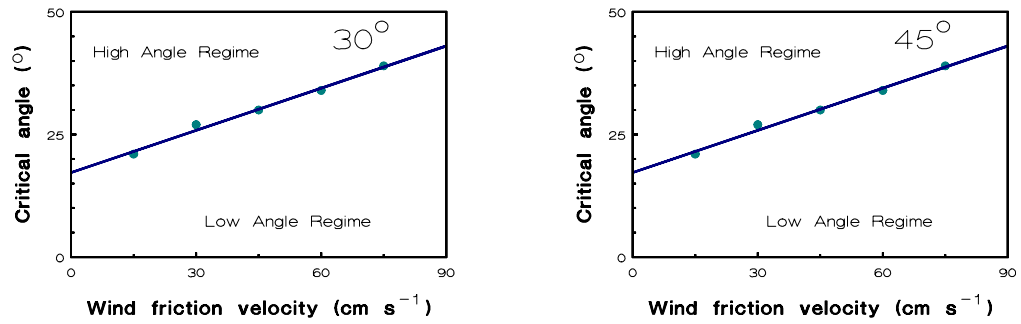

Figure 4. Low and high angle regimes are delineated by a critical angle, which separates azimuthal scans with two maxima per rotation from those with more than two maxima per rotation. Wind directional errors are more likely at lower winds and larger incidence angles.

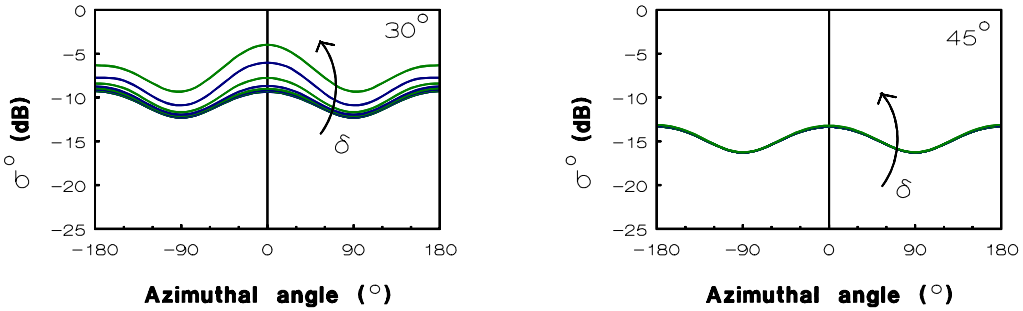

Figure 5. Azimuthal scans for *nonfully developed* seas, i.e., δ ranging from 0.004 to 0.012, by 0.002 increments. This is a moderate wind with $u_* = 30$ cm s^{-1}. The variability of σ^0 attributable to δ is apparent at 30^0 incidence angle.

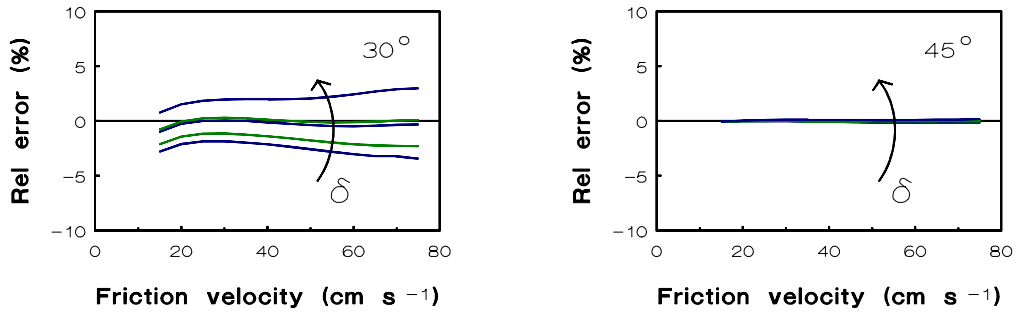

Figure 6. Wind speed errors for *nonfully developed* seas. u_* and δ are as in figure 5. For these conditions, errors due to δ variability are always less than ±10%; so δ effects are small for rising and falling seas with long waves aligned with the wind.

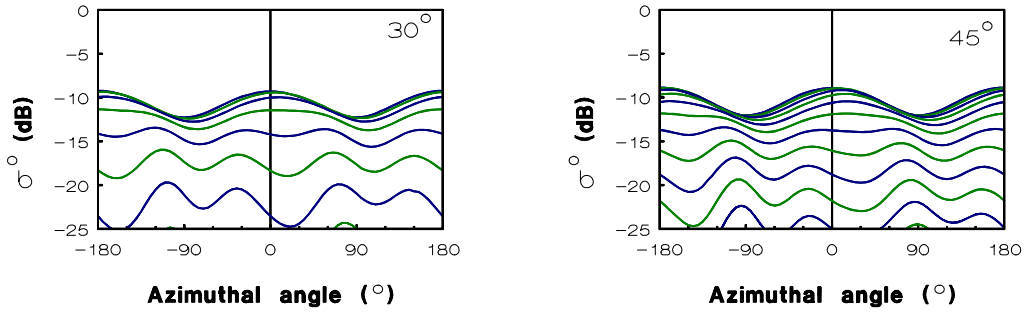

Figure 7. Veering wind effects ensuing *nonfully developed* seas. This falling sea case is for u* = 30 cm s $^{-1}$, δ = 0.004 and Ω increments of 5º. Veering effects can be large, even though the long waves are not very steep.

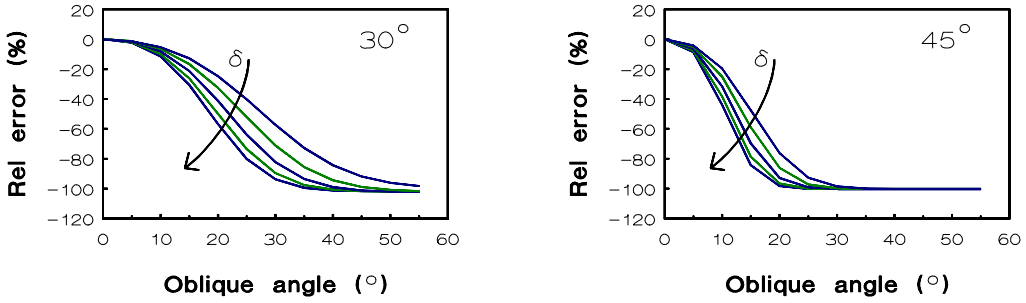

Figure 8. Wind speed errors due to veering winds ensuing *nonfully developed* seas. u_* and δ are as in figure 5. For the entire range of δ, substantial errors develop at both incidence angles. Thus long wave alignment is a concern for all sea states.

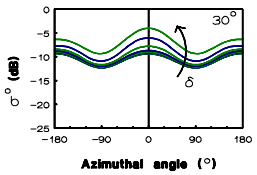
0
−5
−10
−15
−20
−25
−180
−90
0
90
180
30°
δ
Azimuthal angle (°)